

Joy & Dave

Radiative forcing of the stratosphere by  $\text{SO}_2$  gas, silicate ash, and  $\text{H}_2\text{S}$   $\text{O}_4$  aerosols shortly after the 1982 eruptions of El **Chichon**

M. F. Gerstell

California Institute of Technology, Pasadena, California

Joy Crisp and David Crisp

Jet Propulsion Laboratory,

California Institute of Technology, Pasadena, California

Resubmitted to *J. Climate* September 10, 1994.

## ABSTRACT

The 1982 eruptions of El Chichon Volcano injected large quantities of sulfur dioxide gas and silicate ash into the stratosphere. Several studies have shown that the long-lived sulfuric acid aerosols derived from these volcanic effluents produced measurable changes in the radiative heating rates and the global circulation. The radiative and dynamical perturbations associated with the short-lived, but more-strongly-absorbing sulfur dioxide and ash clouds have received much less attention. We therefore used an atmospheric radiative transfer model and observations collected by satellites, aircraft, and ground-based observers to estimate the amplitudes of the stratospheric radiative heating rate perturbations produced by each of these components during the first few weeks after the El Chichon eruption. One week after the April 4, 1982 eruption, net radiative heating rate perturbations exceeding 20 Kelvin per day were found at altitudes near 26 km. The absorption of sunlight by the silicate ash accounts for the majority of this heating. The sulfur dioxide gas and sulfuric acid aerosols each produced net heating perturbations that never exceeded 2 Kelvin per day. In spite of the intense heating by the ash, observations indicate that stratospheric temperatures never increased by more than a few degrees Kelvin. We therefore concluded that this radiative heating was largely balanced by upwelling and adiabatic cooling. The amplitude and spatial extent of this upwelling was estimated with a diagnostic, two-dimensional dynamical model. The ash heating rates may have been balanced by a global enhancement in the stratospheric meridional circulation, with zonally-averaged upward velocities of about 1 cm/sec near the latitude of the plume. This enhanced strato-

spheric circulation persisted only for a few weeks, but it may have played a major role in the vertical and horizontal dispersal of the plume. The vertical transport needed to balance the heating by sulfur dioxide gas was only 5 to 10 percent as large, but this perturbation may have produced a 2-km increase in the altitude of the plume. These results suggest that the radiative forcing by the ash and the sulfur dioxide gas should be included in more comprehensive models of the plume evolution. They also suggest that particle size distributions inferred from ash fallout rates could be wrong if the upwelling associated with this radiative heating is not considered.

## 1. Introduction

Volcanic eruptions can inject large quantities of sulfur-bearing gases and silicate ash into the stratosphere. The sulfur gases (primarily  $\text{SO}_2$  and  $\text{H}_2\text{S}$ ) are the precursors of long-lived volcanic sulfate aerosols, whose effects on the stratospheric thermal structure and dynamics, and the tropospheric climate have been studied extensively (Angell and Korshover, 1983; Dutton and Christy, 1992; Fujita, 1985; Hansen *et al*, 1978; Wang and Lacis, 1978; Kiehl and Briegleb, 1993; Labitzke, Naujokat and McCormick, 1983; Newell, 1970; Parker and Brownscombe, 1983; Quiroz, 1983; Rind *et al*, 1992). A typical finding is that the radiative and dynamical forcing by the aerosols produces warming in the lower stratosphere on a time scale of months, with cooling of the tropospheric climate after a longer period, if the aerosols persist. The silicate ash and  $\text{SO}_2$  gas injected into the stratosphere by a major volcanic eruption should also produce significant changes in the radiative forcing, because these constituents are more effective absorbers of solar and thermal radiation than the sulfuric acid aerosols. The radiative and dynamical effects of ash and  $\text{SO}_2$  at stratospheric levels has received little attention, because unlike the  $\text{H}_2\text{SO}_4$  aerosols, which can persist for years, the stratospheric residence time of these constituents is usually limited to weeks or a few months. The radiative and dynamical forcing by these constituents is therefore unlikely to have a long-term impact on the tropospheric or stratospheric climate. This forcing could still have a significant influence on the early evolution and dispersal of the volcanic plume. Observations acquired soon after the 1982

eruptions of El Chichon Volcano provide the data needed to assess the relative effects of the ash,  $\text{SO}_2$ , and  $\text{H}_2\text{SO}_4$  aerosols on the stratospheric radiative heating rates and circulation. El Chichon Volcano ( $17.3^\circ\text{N}$ ,  $93.2^\circ\text{W}$ ) erupted several times during March and April, 1982. The final and largest eruption occurred on April 4. Vupputuri and Blanchet (1984) and Pollack and Ackerman (1983) estimated maximum stratospheric solar heating rates of 4.5 to 7.5 K/day for the silicate ash from El Chichon, but their study focused on a period extending 3 to 6 months after the eruption, when the majority of the ash had fallen out of the stratosphere. In the present study, we used a comprehensive atmospheric radiative transfer model to estimate the solar and thermal radiative effects of silicate ash and the  $\text{SO}_2$  gas for conditions like those observed during the first month after the April 1982 eruption of El Chichon Volcano, before the  $\text{H}_2\text{SO}_4$  aerosol cloud fully developed. These effects were compared to those produced by the fully-developed  $\text{H}_2\text{SO}_4$  cloud. We found that even though the  $\text{SO}_2$  and ash produced stratospheric heating perturbations that were short-lived and more localized than those caused by the  $\text{H}_2\text{SO}_4$  aerosols, their radiative forcing immediately after the eruption was sufficiently intense to have a strong influence on the vertical and horizontal dispersal of the volcanic plume. In the densest regions of the volcanic plume, at altitudes near 26 km, the solar radiative heating by the ash may have been an order of magnitude stronger than that by  $\text{SO}_2$  gas (or the fully-developed  $\text{H}_2\text{SO}_4$  aerosol cloud), and more than 20 times larger than the background net radiative heating in the lower stratosphere. In spite of this intense heating, no large temperature increases were observed within the plume (Angell and Korshover, 1983). We therefore concluded that the strong radiative heating was largely balanced by the adiabatic expansion

and cooling associated with enhanced upwelling. The intensity and spatial extent of the upwelling needed to balance this heating perturbation was estimated with a stratospheric meridional circulation model based on the Eulerian-mean residual formulation (Santee and Crisp, 1994). The derived upward velocities within the densest part of the plume were comparable to the average fall speeds of the ash particles. Thus, distributions of ash size or density inferred from theoretical fall velocities are likely to be wrong if the buoyancy associated with direct solar heating of the ash is neglected.

Section 2 describes the meridional circulation model, radiative transfer model, and background climatologies adopted here. Section 3 shows the perturbations of stratospheric net heating rates and the circulation needed to balance the direct radiative forcing by the sulfate aerosols. These results provide a comparison standard for the heating by the  $\text{SO}_2$  gas and silicate ash. Section 4 quantifies the radiative effects of the  $\text{SO}_2$ , and Section 5 quantifies the radiative effects of the silicate ash. Section 6 is a summary of our findings.

## 2. Model descriptions

### (a) Radiative transfer model

The computation of net radiative heating and cooling rates requires a detailed representation of the flux distribution throughout the atmosphere. Crisp (1986, 1989, 1990) has developed fast, accurate methods for finding radiative fluxes and heating rates in scattering and absorbing planetary atmospheres. These methods have been combined in a comprehensive radiative transfer model that accommodates all radiative processes known to be important in the terrestrial atmosphere, including absorption, emission, and multiple

scattering by gases and airborne dust particles.

A multiple-scattering model based on the multi-level ~~delta~~-Eddington/adding method (Crisp, 1986) ~~was~~ used to find solar fluxes and heating rates in a **vertically-inhomogeneous**, plane-parallel atmosphere. Because this approach for evaluating the equation of transfer assumes that Beer's law is satisfied at all points along the **optical** path (i.e. the optical depth varies linearly with absorber amount ) it is strictly valid only in spectral regions **sufficiently** narrow that the optical properties do not vary substantially across each. This method should therefore provide reliable results in moderately-wide spectral intervals at ultraviolet and visible wavelengths, where extinction (absorption and scattering) is contributed by airborne ash,  $\text{H}_2\text{SO}_4$  aerosols, Rayleigh scattering, and electronic or photolytic absorption bands of gases ( $\text{H}_2\text{O}$ ,  $\text{CO}_2$ ,  $\text{O}_3$ ,  $\text{N}_2\text{O}$ ,  $\text{CO}$ ,  $\text{CH}_4$ ,  $\text{O}_2$ ,  $\text{SO}_2$ ,  $\text{NO}_2$ ), since the optical properties of these constituents varies slowly with wavelength. This method is also valid in near-infrared spectral regions occupied by very weak water and carbon dioxide lines, whose cores are not saturated for realistic atmospheric optical paths.

This approach for evaluating the equation of transfer is not strictly valid within broad spectral regions occupied by strong near-infrared gas vibration-rotation bands, because the gas absorption coefficients vary rapidly with wavelength in these intervals, and the broadband absorption does not satisfy Beer's law. For these spectral regions, we tested two approaches for evaluating the equation of transfer. In the first, we returned to the two-stream **nonscattering** model described by Crisp (1990). The broadband gas absorption within vibration-rotation bands was evaluated using a Voigt quasi-random model (Crisp, 1990; Santee and Crisp, 1994).  $\text{H}_2\text{SO}_4$  aerosol and silicate ash absorption was also included

at these wavelengths (by adding the aerosol and ash absorption optical depth to that of the gas), but multiple scattering was neglected. In the second approach, we simply ignored the violation of Beer's law and used the multiple scattering model. To estimate the absorption by gases in this model, the Voigt quasi-random model was first used to evaluate the gas transmission between the top of the atmosphere and each atmospheric level in 20 to 200  $\text{cm}^{-1}$  wide spectral regions. These transmission values were then inverted to yield the effective wavelength-averaged gas optical depth in each atmospheric layer. These results were combined with the gas continuum and aerosol absorption optical depths to yield the total absorption optical depth. Finally, the absorption optical depths were combined with the Rayleigh and aerosol scattering optical depths to yield the total extinction optical depth and single scattering albedo in that spectral interval (cf. Crisp, 1986). These two methods were tested against rigorous line-by-line multiple scattering calculations performed with a multi-stream discrete ordinate model (Stamnes *et al*, 1988; Bell and Crisp, 1993). Both approximate methods produced similar results for clear-sky conditions, with heating rate errors rarely exceeding 5%. The second method usually produced fluxes and heating rates that were more accurate for cloudy or aerosol-laden atmospheres. We therefore selected the second approach for the calculations presented here. The thermal radiative transfer model used here includes absorption by gases and the absorption by airborne ash and aerosols, but neglects multiple scattering. This simplified approach was adopted because the single-scattering albedos of the  $\text{H}_2\text{SO}_4$  aerosol and ash particles are small ( $\leq 0.2$ ) at thermal wavelengths. The Voigt quasi-random model (Crisp 1989, 1990) is used to find the broadband gas transmission functions in spectral intervals that were 2  $\text{cm}^{-1}$  wide.



The solution to the equation of transfer is identical to that described in Crisp (1989), equations (5)–(9), except that we have added the surface boundary condition given in Crisp (1990, equation 14). The atmosphere was resolved into 60 vertical layers between the surface, at 1013 mbar, and the 0.178 mbar level. The levels defining the boundaries of each layer were equally spaced in the logarithm of pressure and characterized by a pressure, a temperature, the gas mixing ratios for eight gases, ( $\text{H}_2\text{O}$ ,  $\text{CO}_2$ ,  $\text{O}_3$ ,  $\text{N}_2\text{O}$ ,  $\text{CH}_4$ ,  $\text{O}_2$ ,  $\text{NO}_2$ ,  $\text{SO}_2$ ) and the optical thickness for each of aerosol particle type ( $\text{H}_2\text{O}$ ,  $\text{H}_2\text{SO}_4$ , silicate ash). The aerosol particle number density was assumed to be constant within each layer. The temperatures and gas mixing ratios were assumed to vary linearly with log pressure between the top and bottom of each layer. The solar spectrum was divided into 755 spectral intervals between 0.125 and 5.26  $\mu\text{m}$  to resolve the wavelength dependence of the solar flux and that of gas and dust absorption features. The spectrally-dependent solar fluxes above the atmosphere at wavelengths between 0.125 and 0.8  $\mu\text{m}$  are those of the World Meteorological Organization (1986); outside this wavelength range we used the data of Thekaekara (1969). The thermal spectrum was divided into 95 spectral intervals between 5.26 and 200  $\mu\text{m}$  to resolve the wavelength dependence of the Planck function and various gas and aerosol absorption bands. Spectral intervals occupied by infrared gas vibration-rotation bands were further subdivided into  $2\text{-cm}^{-1}$  intervals to improve the accuracy of the multiplicative property of narrow-band transmission (Goody and Yung, 1989), which is used to combine the effects of two or more gases that absorb in the same spectral interval.

The absorption line parameters for gases at infrared wavelengths were taken from

the 1992 edition of the HITRAN database (Rothman *et al*, 1992). The gas absorption cross sections at ultraviolet and visible wavelengths were taken from DeMore *et al* (1992). Wavelength-dependent extinction, absorption, and scattering cross-sections and scattering phase functions for liquid water droplets, H<sub>2</sub>SO<sub>4</sub> aerosols, and silicate ash particles were derived from the refractive index data for these aerosols with a model that incorporates the Mie-scattering algorithm of Wiscombe (1980; personal communication, 1992), with the methods for integrating over particle size distributions described by Hansen and Travis (1974). The wavelength-dependent refractive indices for liquid water were taken from Hale and Querry (1973). Cloud particle size distributions for altostratus and stratus clouds were taken from Hansen (1971). Because Mie scattering is not appropriate for evaluating the optical properties of the non-spherical ice particles that compose cirrus clouds, we adopted published values of the wavelength-dependent optical properties of columnar ice crystals (Freeman and Lieu, 1979). For the H<sub>2</sub>SO<sub>4</sub> aerosols, the real and imaginary components of the wavelength-dependent refractive index of 75% sulfuric acid solution were taken from Palmer and Williams (1975). A single log-normal size distribution (cf. Eqn. (2.60) of Hansen and Travis, 1974) was used at all latitudes. The geometric mean particle radius ( $r_g$  in Hansen and Travis, 1974) was assumed to be 0.4  $\mu\text{m}$ , and the geometric standard deviation with respect to the natural logarithm of particle radius ( $u$  in Hansen and Travis, 1974) was assumed to be 0.34  $\mu\text{m}$  (cf. Pollack *et al*, 1991; Bandeen and Fraser, 1982; Oberbeck *et al*, 1983). The Chichon ash was composed of andesitic glass and crystals (MacKinnon *et al*, 1984). For our calculations, we used the optical properties of crystalline andesite (Pollack *et al*, 1973). Sensitivity experiments on rhyolite and basalt

glasses suggest that omitting the optical properties of the andesite glass may produce net radiative heating rates that are up to 20% too large, but the optical properties of andesitic glass were not available. The nominal mean radius of the stratospheric ash particles was assumed to be  $3\text{ }\mu\text{m}$  one week after the eruption. Alternate distributions with mean radii of 1 and  $5\text{ }\mu\text{m}$  were also used. These particle radii are roughly consistent with aircraft observations, which indicate a median radius of  $6\text{ }\mu\text{m}$  as late as May 7, for all collected particles larger than  $2\text{ }\mu\text{m}$  (MacKinnon *et al*, 1984). The geometric standard deviations of all ash size distributions, with respect to the natural logarithm of the radius, were assumed to be  $\sigma=0.16$ , consistent with measurements of the ash acquired in September, 1982 (Oberbeck *et al*, 1983).

This radiative transfer model was used to find the diurnally-averaged solar heating rates, thermal cooling rates, and net radiative heating rates at 19 latitudes including the poles, with an increment of  $10^\circ$  of latitude. The solar fluxes and heating rates for each latitude were evaluated at four solar zenith angles, and these results were integrated over the solar day to obtain the diurnally-averaged solar heating rates. Thermal radiances were obtained for two streams (one up, one down); a diffusivity factor of 1.66 (Elsasser, 1943) was used to obtain the upward and downward thermal fluxes and cooling rates at each model level. Finally, the net heating rates at each latitude and altitude were obtained by differencing the solar heating rates and thermal cooling rates.

#### (b) Meridional circulation model

Given estimates of the thermal structure and net radiative heating rates at stratospher-

ic levels, the net meridional transport can be derived diagnostically from the transformed Eulerian-mean (TEM) equations of motion (Andrews and McIntyre, 1976; Dunkerton, 1978; Shia *et al.*, 1989; Santee, 1992). This approach is widely used in stratospheric chemical tracer transport studies, because it incorporates the almost equal, but opposing, effects on planetary scale waves and the zonal-mean meridional circulation, to yield a direct estimate of the net, Lagrangian-mean mass and heat transports. This approach is most valid at altitudes within the middle and lower stratosphere, where the waves are approximately linear and time-invariant. In the TEM approach, the residual, zonal-mean meridional and vertical velocities,  $v^*$ ,  $w^*$ , are defined through the transformation:

$$v^* \equiv \bar{v} - \frac{1}{\rho} \frac{\partial}{\partial z} \left( \frac{\rho \overline{v'T'}}{\frac{\partial \bar{T}}{\partial z} + \frac{g}{c_p}} \right) \quad (1)$$

$$w^* \equiv \bar{w} + \frac{1}{a \cos \phi} \frac{\partial}{\partial \phi} \left( \frac{\overline{\psi'T'} \cos \phi}{\frac{\partial \bar{T}}{\partial z} + \frac{g}{c_p}} \right), \quad (2)$$

where  $\bar{v}$  and  $\bar{w}$  are the zonal-mean velocity components in the meridional and vertical directions, respectively,  $a$  is the radius of the earth,  $z$  the log-pressure altitude,  $\rho$  is the atmospheric density,  $g$  is the gravitational acceleration,  $\phi$  is latitude, and  $c_p$  is the specific heat at constant pressure. The  $\overline{v'T'}$  term describes the eddy heat flux. When these definitions are substituted into the zonally-averaged primitive equations, the mass continuity and thermodynamic energy equations take the form [Andrews, Holton, and Leovy, 1987]:

$$\frac{1}{a \cos \phi} \frac{\partial}{\partial \phi} (v^* \cos \phi) + \frac{1}{\rho} \frac{\partial}{\partial z} (\rho w^*) = \frac{\partial \rho}{\partial t} \approx 0 \quad (3)$$

$$\frac{\partial \bar{T}}{\partial t} + \frac{v^*}{a} \frac{\partial \bar{T}}{\partial \phi} + w^* \left[ \frac{\partial \bar{T}}{\partial z} + \frac{g}{c_p} \right] - \bar{Q} = -\frac{1}{\rho} \frac{\partial}{\partial z} \left[ \frac{\rho \overline{v'T'} \frac{\partial \bar{Q}}{\partial \phi}}{a \left( \frac{\partial \bar{T}}{\partial z} + \frac{g}{c_p} \right)} + \rho \overline{w'T'} \right]. \quad (4)$$

where  $H$  is a mean scale height,  $\bar{T}$  is the zonal-mean temperature, and  $Q$  is the zonal-mean (diurnally-averaged) net diabatic heating rate. The term on the right-hand side of the thermodynamic energy equation (Eq. 4) is called the ‘wave heating’ term. This term vanishes for quasi-geostrophic motions, and for steady, conservative gravity waves, and is usually neglected. In addition, at stratospheric levels, radiative heating and cooling rates dominate the net diabatic heating, so that  $Q$  reduces to the net radiative heating. Finally, if we neglect  $d\rho/dt$  and  $d\bar{T}/dt$  in Eqs. 3 and 4, these two equations can be solved simultaneously in terms of the steady-state TEM streamfunction,  $\psi$  (Shia *et al*, 1989):

$$\left(\frac{\psi}{H} - \frac{\partial\psi}{\partial z}\right) \frac{\partial\bar{T}}{\partial\phi} + \left(\frac{\partial\bar{T}}{\partial z} + \frac{g}{c_p}\right) \frac{\partial\psi}{\partial\phi} = \bar{Q} a \cos \phi. \quad (5)$$

This equation describes the net steady-state meridional circulation that transports enough heat to maintain the observed thermal structure in the presence of the imposed net radiative heating rate. It should be interpreted as a diagnostic statement of balance, rather than a mechanistic model of the processes producing the circulation. In other words, even though this equation describes a circulation consistent with the observed radiative heating field, it does not require that the circulation be forced directly by that heating. In many studies (e.g., Dunkerton, 1978; Rosenfield *et al*, 1987; Gille *et al*, 1987), Eq. 4 is simplified further by neglecting the second term on the left-hand side, which accounts for horizontal advection of heat. The thermodynamic energy equation then reduces to the form:

$$w^* \left[ \frac{\partial\bar{T}}{\partial z} + \frac{g}{c_p} \right] \approx \bar{Q}. \quad (6)$$

This approximation was not adopted here, but the simple expression in Eq. 6 more

clearly illustrates the linear relationship between the TEM vertical velocity,  $w^*$ , and the net radiative heating rates,  $\bar{Q}$ . The numerical methods used to solve Eq. 5 are described in detail in Santee (1993) and Santee and Crisp (1994).

(c) Background atmospheres and surfaces

The fractional cloudiness and cloud-top pressures for tropospheric water clouds were derived by averaging the 1984-86 values for each latitude and month as reported by the International Satellite Cloud Climatology Project (ISCCP; see Rossow and Schiffer, 1991). ISCCP data are not available for 1982, the year of El Chichon's eruption. All high clouds were modeled as cirrus clouds composed of ice crystals, with an optical thickness of 1.5 at 0.425  $\mu\text{m}$ ; all middle-altitude clouds were assumed to be altostratus, with an optical thickness 5 at 0.425  $\mu\text{m}$ ; all low-level clouds were modeled as stratus with an optical thickness of 10 at 0.425  $\mu\text{m}$ .

Climatological temperature profiles at each latitude for April and July were obtained by averaging National Meteorological Center (NMC) data collected in 1984-86 (Gelman *et al*, 1986). Eight absorbing gases were included in our background atmospheres. The volume mixing ratios of  $\text{O}_2$  and  $\text{CO}_2$  were assumed to be constant, at 0.21 and 0.00033. Climatological  $\text{O}_3$  profiles were obtained by averaging the Solar Backscatter Ultraviolet (SBUV) data from 1984-1986 for each latitude and month. The 1984-86 period was chosen for consistency with available ISCCP data, even though NMC and SBUV data from the Chichon period could have been used. Stratospheric  $\text{O}_3$  abundances in the south polar regions, where SBUV data were not available, were obtained from the 1986 balloon data

described by Kurylo *et al* (1989). Stratospheric profiles of  $\text{H}_2\text{O}$ ,  $\text{N}_2\text{O}$ ,  $\text{CH}_4$ , and  $\text{NO}_2$  for each latitude and month were derived from Nimbus-7 LIMS and SAMS measurements and (for  $\text{H}_2\text{O}$ ) ground-based microwave data. The sulfur dioxide profile for the unperturbed atmosphere was taken from Warneck (1988, Fig. 3-13). Tropospheric  $\text{H}_2\text{O}$  mixing ratios were derived from climatological specific humidity data (Oort, 1983). The mixing ratios of other gases at tropospheric levels were estimated by extrapolating stratospheric values to the surface, assuming the logarithm of the mixing ratio decreased linearly with the logarithm of pressure.

Surface albedos at visible wavelengths for each latitude and month were also taken from the ISCCP database. At near-infrared wavelengths, we adopted the approach described by Briegleb (1992) and assumed that the ratio of near-infrared albedo to visible albedo depends on surface type (snow, ice, water, vegetation, etc.). Meridional distributions of 12 surface types were obtained from the Goddard Institute for Space Studies database (see Matthews, 1983). The visible albedos given by ISCCP were extrapolated into the ultraviolet, to 0.2  $\mu\text{m}$ , and set to zero at shorter wavelengths. Surface albedos at thermal infrared wavelengths were assumed to be zero for dry land. For snow, values were taken from Warren (1982). For the ocean, the albedos were calculated directly from the optical constants of seawater, with the aid of a Fresnel facet model for rough surfaces. This model explicitly includes the effects of increased sea-surface roughness as one goes from the tropics to high latitudes.

### 3. Sulfuric Acid Aerosols

Net radiative heating rates and diabatic streamfunctions were derived for two reference atmospheres. The first included only the climatological gas and cloud distributions described in the previous section. The second used this background climatology, but also included an  $\text{H}_2\text{SO}_4$  aerosol cloud with latitude-dependent column optical depths similar to those measured by the Solar Mesosphere Explorer (SME) several months after the eruption of El Chichon (see Eparvier *et al*, 1994; Thomas *et al*, 1983). The same aerosol vertical profile was used at all latitudes. This profile was derived from observations acquired near  $20^\circ\text{N}$  in early July, 1982. It assumes a Gaussian distribution of spherical particles with number densities peaked at 26 km, and a half-width-at-half-max of 1.5 km (DeLuisi *et al*, 1983; Shibata *et al*, 1984; Oberbeck *et al*, 1983; Labitzke *et al*, 1983).

The diurnal-average net radiative heating profile at  $20^\circ\text{N}$  for the background climatology and the  $\text{H}_2\text{SO}_4$  aerosol-laden atmosphere are shown in Fig. 1a. The net radiative heating by the aerosols is most intense at the 26 km level, at latitudes between the equator and  $40^\circ\text{N}$ , where the aerosols are most concentrated. The solar and thermal contributions to the net heating by the  $\text{H}_2\text{SO}_4$  aerosol clouds are compared in Figure 1b. These results confirm the findings of other investigators (Young *et al*, 1994, and its references), that the radiative perturbation by  $\text{H}_2\text{SO}_4$  aerosol is mainly due to the absorption of upwelling thermal radiation emitted by the surface and lower troposphere. The majority of the absorption of solar radiation by the  $\text{H}_2\text{SO}_4$  aerosols occurs at wavelengths longer than 3  $\mu\text{m}$ , where these aerosols have very low single scattering albedos.

The net radiative heating by the  $\text{H}_2\text{SO}_4$  aerosols never exceeds 2 K/day, but this heating could still produce significant stratospheric temperature increases over the lifetime



of the aerosol cloud if it were not balanced by horizontal or vertical transport. The amplitude of the transport needed to balance this heating was estimated with the TEM model described in Section 2.2. The derived stratospheric **streamfunctions** for the baseline **climatology** and the aerosol-laden atmospheres are compared in Figs. 2a and 2b. We found that the net heating by the aerosols could be balanced by intensified **upwelling** ( $\approx 0.5$  mm/s) at low latitudes near 26 km altitude, where the aerosol concentrations and heating rates are largest. This upwelling is associated with the formation of a weak meridional circulation cell in the northern hemisphere.

#### 4. Sulfur Dioxide Gas

The similarity between  $\text{SO}_2$  and  $\text{O}_3$  absorption spectra at ultraviolet wavelengths (Fig. 3) suggests that volcanic  $\text{SO}_2$  should produce significant perturbations of the solar heating rates. The largest heating rate perturbations should occur where the  $\text{SO}_2$  concentrations exceed the ozone concentrations, as they did near the center of El Chichon's eruption plume. The Total Ozone Mapping Spectrometer (TOMS) acquired approximately 100,000 measurements of the  $\text{SO}_2$  column abundances each day (Krueger, 1983). We used the TOMS data for April 4, 5, 6, 12, 19, and 26, 1982. The  $3^\circ$  by  $3^\circ$  field of view of this instrument is stepped to 35 cross-track positions every 8 seconds as the spacecraft follows a sun-synchronous, noon-midnight polar orbit. The spatial resolution at the nadir is 50 by 50 km, and increases to 150 by 300 km at the far scan positions. Krueger (1983) estimated average  $\text{SO}_2$  column amounts near 42 Dobson units (DU) inside a volcanic cloud whose area was  $3.3 \times 10^6$  km<sup>2</sup> on April 6, 1982. Peak  $\text{SO}_2$  column amounts of 750 DU were

observed during the 24 hours immediately following the April 4, 1982 eruption.

We performed a series of sensitivity tests to quantify the effects of  $\text{SO}_2$  absorption on the net heating rates. In these tests, we assumed that the  $\text{SO}_2$  was concentrated in a plume with a Gaussian vertical profile, with a vertical half-width-at-half-max of 1.5 km. Even though  $\text{SO}_2$  absorbs strongly at both solar and thermal wavelengths, its effect on the net radiative heating is dominated by the absorption of sunlight. For a given  $\text{SO}_2$  column abundance, the solar heating rate perturbation increased as the altitude of the peak of the  $\text{SO}_2$  plume increased (Fig. 4). The maximum solar heating rates were produced when the maximum  $\text{SO}_2$  concentrations were near 30 km, where this gas begins to escape the shading by the  $\text{O}_3$ . When the peak  $\text{SO}_2$  concentrations occur at higher altitudes, the absorption of sunlight by this gas continues to increase, but the total heating peak is reduced, because ozone absorption no longer contributes much to the total heating.

Just after the April 4, 1982 eruption of El Chichon, the largest  $\text{SO}_2$  concentrations probably occurred within the ash cloud. This cloud was centered near 26 km altitude on April 10 (DeLuisi *et al.*, 1983). The amplitude of the heating rate perturbation produced at this altitude for a 42 DU sulfur dioxide layer was slightly larger than that produced by the  $\text{H}_2\text{SO}_4$  aerosol layer described in the previous section. The large  $\text{SO}_2$  abundances extended over a much more limited area than the  $\text{H}_2\text{SO}_4$  aerosols, however. If the derived  $\text{SO}_2$  radiative forcing were averaged over a  $10^\circ$  wide zonal band, and used to create an analog of Fig. 2b, the resulting streamfunction would be almost indistinguishable from that obtained in the unperturbed case.

In spite of their limited spatial extent,  $\text{SO}_2$  concentrations as large as those seen near

the center of the El Chichon plume could have a considerable effect on the height of the volcanic plume. To illustrate this, Eq. 6 can be rearranged to yield an expression for the elevation change,  $\Delta Z$ , associated with the net heating,  $Q$ :

$$\Delta Z = S^{-1} \int Q dt, \quad (7)$$

where  $t$  is time  $Q$  the radiative heating rate, and  $S (= dT/dz + g/C_p)$  is about 12 K/km at 26 km altitude, at 20° N in the springtime.

The amplitude of the radiative heating for an  $\text{SO}_2$  plume centered at 25-26 km altitude is shown as a function of the  $\text{SO}_2$  column amount in Fig. 5. The lower curve shows the amplitude of the heating rate perturbation for this latitude, altitude, and season calculated with respect to a background atmosphere with an unperturbed  $\text{SO}_2$  abundance. Maximum  $\text{SO}_2$  column amounts in the TOMS data were approximately 750, 200, 50, and 30 DU on April 4, 6, 12, and 26 respectively. Using these values, and integrating Eq. 7 over time, we find  $\Delta Z$  for that part of the atmosphere where the  $\text{SO}_2$  concentration are largest to be about 2 km during April—doubling the rise due to the Brewer-Dobson circulation at this latitude and season.

Another way to assess the magnitude of the radiative forcing by  $\text{SO}_2$  gas is to compare the total energy it transfers into the 23-27 km layer to that deposited in the atmosphere by the erupted volcanic solids. A rough upper limit on the latter is 0.8 EJ (1 EJ =  $10^{18}$  J), using an estimate of 0.4 km<sup>3</sup> magma (Rampino *et al*, 1988), magma density of 2600 kg m<sup>-3</sup>, a heat capacity of 1000 J kg<sup>-1</sup> K<sup>-1</sup> (Peck, 1978), a magma temperature of 810°C (Rye *et al*, 1984; Luhr, 1990), which cools to about 20°C since most of it remains near the

ground or quickly falls back to the ground, in the tropics.

The excess solar energy absorbed by the  $\text{SO}_2$  layer, compared to that usually absorbed at this latitude, altitude, and season, can be estimated from the heating rates shown in Fig. 5 (lower curve) and the TOMS  $\text{SO}_2$  maps. For April 5, 12, 19, and 26, we find excess energy deposition rates of 0.32, 0.27, 0.14, and 0.03 EJ/day, for a time-integrated total of 4-5 EJ. Thus, the energy collected in the middle stratosphere by the  $\text{SO}_2$  plume during the first few weeks following the eruption may have been at least as great as the energy delivered to the atmosphere by the erupted solids.

## 5. Silicate Ash

DeLuisi *et al* (1983) measured optical depths exceeding 0.7 (at 425 nm) at Mauna Loa on two dates in mid-April, 1982. Because little  $\text{H}_2\text{SO}_4$  aerosol would have formed in the first week after the eruption (e.g., Turco *et al*, 1983), the measured optical thickness was attributed mainly to silicate ash. We therefore adopted an ash optical thickness of 0.6 for the sensitivity tests presented here. We assumed that the ash layer was centered at 26 km, and had a vertical half-width-at-half-maximum of 1.5 km. This is roughly consistent with lidar backscatter observations over Mauna Lea, which revealed a peak at 25 km altitude for a few days following the April 9 arrival of the eruption plume from El Chichon (Coulson *et al*, 1982).

The solar, thermal, and net radiative heating rates produced by this ash layer are shown in Fig 6. We found that this ash plume produces a radiative perturbation that is about an order of magnitude larger than that caused by the  $\text{SO}_2$  gas or the  $\text{H}_2\text{SO}_4$

aerosol plumes described above. The amplitude of the ash heating is very sensitive to the mean particle radius (Fig. 6a), which is uncertain for the eruption of El Chichon. For the nominal  $3\text{-}\mu\text{m}$  distribution, the heating rates can exceed 23 K/day. This radiative perturbation by silicate ash is due mainly to an increase of solar heating, with a smaller contribution from a reduction in thermal cooling (Fig. 6b).

The large radiative heating rates associated with the ash cloud should produce dramatic changes in the stratospheric thermal structure or dynamics. Monthly-averaged NMC temperatures measured at altitudes near 26 km between  $15^{\circ}$ – $25^{\circ}$ N latitude show no variations from climatology larger than about 2 K during April, 1982. We therefore concluded that the ash radiative forcing was largely balanced by changes in the stratospheric circulation. We used the TEM model to estimate the amplitude of these circulation changes. Streamfunctions for background and perturbed stratospheres are compared Fig. 7. The TEM circulation shown in Fig 7b assumes that an ash layer with an optical depth 0.6 circled the globe and extended from  $15^{\circ}$ N to  $25^{\circ}$ N. It is unlikely that this ash cloud covered this entire zonal band, since this would require that more than 1% of the erupted solids (cf. Cadle *et al* 1976) reached the middle stratosphere. However, if such a layer existed at some longitudes, the residual vertical velocity inferred from net diabatic heating (of 23 K/day) at the center of the ash layer would have been about 1 cm/s. The ash therefore produces a much greater short-term perturbation in the stratospheric circulation than the  $\text{H}_2\text{SO}_4$  aerosols or the  $\text{SO}_2$  gas. These large ash effects could play an important role in the dispersal of the volcanic plume in the stratosphere. The time-integrated effects of the ash do not exceed those of the aerosols, however, because the stratospheric residence time

of the ash is much shorter than that of the aerosols.

Large vertical motions like those described above should also affect the ash particle fallout rates. To estimate these rates, we first computed the Stokes fall speeds using molecular viscosities deduced from the monthly-averaged NMC temperature profiles for May, 1982 at 20°N. Results presented in Table I suggest that 3- $\mu\text{m}$  ash particles should fall from 26 km altitude to the tropopause in a week, but this inference ignores two important facts. First, the Stokes formulation assumes spherical particles, which is probably inaccurate. MacKinnon *et al.* (1984) found that a Wilson-Huang formulation of terminal velocity incorporating a shape factor (Wilson and Huang, 1979) gives fall speeds about half as large. Second, the vertical advection associated with the absorption of solar radiation by the silicate ash may actually exceed the Wilson-Huang fall speed for some particle sizes. For example, upward velocities at the center of the ash layer may have been about 1 cm/s. This exceeds the Wilson-Huang fall speed of the 3- $\mu\text{m}$  particles. This upwelling will reduce the ash particle fallout rates, but will not suspend the particles indefinitely for the following three reasons. First, the amplitude of the heating rates and the associated circulation will decrease as the ash cloud is dispersed horizontally by the perturbed circulation. Second, the ash cloud consists of a distribution of particle sizes, and the heating rates will decrease as particles with radii much greater than 3  $\mu\text{m}$  fall out, since the ash heating rate is a strong function of particle size (Fig. 6). Third, the background temperature profiles suggest increasing viscosity against particle fall as the air parcels rise, so that a stable equilibrium position for the particles should not exist. Thus these experiments cannot fully replace other explanations for the unexpected persistence of large particles (Gooding

*et al.*, 1983; Knollenberg and Huffman, 1983).

## 6. Summary

Numerical experiments involving the best accessible data on sulfur dioxide, ash, and sulfate aerosols from the period immediately following the 1982 eruptions of El Chichon have shown that the instantaneous, local radiative forcing by sulfur dioxide gas is comparable to that of the successor sulfuric acid aerosols. The time-averaged, globally integrated effects of the sulfur dioxide are much smaller than those of the aerosols, however, since the  $\text{SO}_2$  has a much shorter stratospheric residence time. In spite of this, the radiative heating by the  $\text{SO}_2$  can contribute to the height of the plume. Furthermore, the solar energy absorbed in the stratosphere by  $\text{SO}_2$  may exceed the energy delivered to the atmosphere by erupted solids.

Silicate ash deposited in the middle stratosphere has a much greater potential than sulfur dioxide to heat or elevate the layer in which it occurs. The amplitude of the ash heating depends strongly on the ash size distribution, which is not well known for El Chichon. To balance the net radiative heating by ash particles, we infer a vertical advection of about 1 cm/s, which is unusual in the stratosphere. No formulation of fall velocities is likely to be valid if the vertical advection associated with the particles' absorption of solar radiation is ignored.

We reiterate the recommendation, published in an earlier abstract (Gerstell *et al.*, 1993), that general circulation models used to study the effects of volcanism on climate should incorporate the radiative forcing of both the  $\text{SO}_2$  and the silicate ash, in addition

to the sulfuric acid aerosols. Our study differs from that of Young *et al* (1994), who performed their calculations for  $\text{H}_2\text{SO}_4$  aerosol even though they used the probable presence of uncoated ash to justify their choice of optical thickness. We find that the possibly large perturbation due to silicate ash is dominated by short-wave heating. While the potential effect of silicate ash on global circulation is more obvious than that of  $\text{SO}_2$  gas, a model that can produce a full three-dimensional prognosis of the plume's evolution will certainly be affected by inclusion of the sulfur dioxide.

For a more accurate assessment of the impact of volcanic ash on the stratospheric thermal structure and dynamics, we need much a much better description of the ash distribution and optical properties. These parameters must be determined in a timely manner since the ash has a limited stratospheric lifetime. The measurements collected just after the April 1982 eruptions of El Chichon still provide one of the best data sets for this purpose. Extensive measurements of the Mt. Pinatubo eruption plume were also made, but these measurements were less appropriate for studying the ash properties because very early lidar observations of its plume are not available. The sensitivity experiments described here would therefore have been even more speculative for the Mt. Pinatubo eruption.

#### Acknowledgements

We thank Ian Sprod and Arlin Krueger for providing TOMS sulfur dioxide data. We thank Frank Eparvier for providing a preprint of his SME aerosol columns. We acknowledge use of the ISCCP-C2 database for 1984-86. We are grateful for the detailed comments of



two anonymous referees.

Support for this study was provided by the NASA Global Change Research Program, the NASA **Volcano-Climate** Interactions Program, and the NASA Upper Atmosphere **Research** Program. The work by J. Crisp and D. Crisp was carried out at the Jet Propulsion Laboratory, California Institute of Technology, under contracts with the National Aeronautics and Space Administration. The work by M. Gerstell was carried out at the California Institute of Technology in partial fulfillment of the requirements for a Ph.D. degree in the Division of Geological and Planetary Sciences, under a contract with the National Aeronautics and Space Administration.

## References

- Andrews, Holton and Leovy, 1987: *Middle Atmosphere Dynamics*. Orlando, FL, Academic Press, 489 pp.
- Andrews, D.G. and M.E. McIntyre, 1976: Planetary waves in horizontal and vertical shear: the generalized Eliassen-Palm relation and the mean zonal acceleration. *J. Atmos. Sci.* 33, 2031-2048.
- Angel, J.K. and J. Korshover, 1983: Comparison of stratospheric warmings following Agung and Chichon. *Mon. Weather Rev.* 111, 2129-2135.
- Bandeem, W.R. and R.S. Fraser (eds.), 1982: Radiative effects of the El Chichon volcanic eruption: preliminary results concerning remote sensing. *NASA Technical Memo* 84959, 102 pp.
- Bell, J.F. and D. Crisp, 1993: Ground-based imaging spectroscopy of Mars in the near-IR: preliminary results. *Icarus* 104, 2-19.
- Briegleb, B. P., 1992: Delta- Eddington approximation for solar radiation in the NCAR community climate model. *J. Geophys. Res.* 97, 7603-7612.
- Cadle, R. D., C.S. Kiang, and J.-F. Louis, 1976: The global scale dispersion of the eruption clouds from major volcanic eruptions. *J. Geophys. Res.* 81, 3125-3132.
- Coulson, K. L., T.J. DeFoor, and J. DeLuisi, 1982: Lidar and optical polarization measurements of stratospheric cloud in Hawaii. *EOS Trans. AGU* 63, 897.
- Crisp, D., 1986: Radiative forcing of the Venus mesosphere, I. Solar fluxes and heating rates. *Icarus* 67, 484-514.
- Crisp, D., 1989: Radiative forcing of the Venus mesosphere, II. Thermal fluxes, cooling

rates, and radiative equilibrium temperatures. *Icarus* 77, 391-413.

Crisp, D., 1990: Infrared radiative transfer in the dust-free Martian atmosphere, *J. Geophys. Res.* 95, 14577-14588.

DeLuisi, J. J., E.G. Dutton, K.L. Coulson, T.E. DeFoor, and B.G. Mendonca, 1983: On some radiative features of the El Chichon volcanic stratospheric dust cloud and a cloud of unknown origin observed at Mauna Loa. *J. Geophys. Res.* 88, 6769-6772.

DeMore, W. B., D.M. Golden, R.F. Hampson, M.J. Kurylo, C.J. Howard, A.R. Ravishankara, C.E. Kolb, and M.J. Molina, 1992: Chemical kinetics and photochemical data for use in stratospheric modeling. *JPL Publication* 92-20, Jet Propulsion Laboratory, Pasadena, CA, 185 pp.

Dunkerton, T., 1978: On the mean meridional mass motions of the stratosphere and mesosphere. *J. Atmos. Sci.* 35, 2325-2333.

Dutton, E.G. and J.R. Christy, 1992: Solar radiative forcing at selected locations and evidence for global lower tropospheric cooling following the eruptions of El Chichon and Pinatubo. *Geophys. Res. Lett.* 19, 2313-2316.

Elsasser, W. M., 1943: Heat transfer by infrared radiation in the atmosphere. *Harvard Meteorological Studies, No. 6*. Harvard University Press.

Eparvier, F., D.W. Rusch, R.T. Clancy, and G.E. Thomas, 1994: Solar Mesosphere Explorer satellite measurements of El Chichon stratospheric aerosols 2: aerosol mass and size parameters. Submitted to *J. Geophys. Res.*

Freeman, K.P. and K.N. Lieu, 1979: Climate effects of cirrus clouds. *Adv. Geophys.* 21, 231-287.

Fujita, T., 1985: The abnormal temperature rises in the lower stratosphere after the 1982 eruptions of the volcano El Chichon, Mexico. Papers in *Meteor. and Geophys.* **36**, 47--60.

Gelman, M. E., A. J. Miller, K. W. Johnson and R. M. Nagatani, 1986: Detection of long term trends in global stratospheric temperature from NMC analyses derived from NOAA satellite data. *Adv. Space Res.* **6**, 17-26.

Gerstell, M.I?., J. Crisp and D. Crisp, 1993: Radiative forcing of the stratosphere by  $\text{SO}_2$ , ash, and  $\text{H}_2\text{SO}_4$  aerosols, during the first 3 months after the El Chichon eruptions. *EOS Trans. AGU* **74:43**, 105.

Gille, J. C., L.V. Lyjak, and A.K. Smith, 1987: The global residual mean circulation in the middle atmosphere for the northern winter period. *J. Atmos. Sci.* **44**, 1437-1452.

Gooding, J.L. anti U.S. Clanton, 1983: El Chichon volcanic ash in the stratosphere: Particle abundances and size distributions after the 1982 eruption. *Geophys. Res. Lett.* **10**, 1033-1036.

Goody, R.M. and Y.L. Yung, 1989: *Atmospheric Radiation: Theoretical Basis*, Chap. 4. New York, Oxford University Press, 519 pp.

Hale, G.M. and M.R. Querry, 1973: Optical constants of water in the 200-nm to 200- $\mu\text{m}$  wavelength region. *Appl. Optics* **12**, 555-563.

Hansen, J. E., 1971: Multiple scattering of polarized light in planetary atmospheres. Part II: Sunlight reflected by terrestrial water clouds. *J. Atmos. Sci.* **28**, 1400-1426.

Hansen, J.E. and L.D. Travis, 1974: Light scattering in planetary atmospheres. *Space Sci. Rev.* **16**, 527-610.

Hansen, J. E., W.-J. Wang, and A.A. Lacis, 1978: Mount Agung eruption provides test of a global climatic perturbation. *Science* 199, 1065-1068.

Kiehl, J.T. and B.P. Briegleb, 1993: The relative roles of sulfate aerosols and greenhouse gases in climate forcing. *Science* 260, 31 1-314.

Knollenberg, R.G. and D. Huffman, 1983: Aerosol measurements in El Chichon. *Geophys. Res. Lett.* 10, 1025-1028.

Komhyr, W. D., R.D. Grass and P.J. Reitelbach, 1989: Total ozone, ozone vertical distributions, and stratospheric temperatures at South Pole, Antarctica in 1986 and 1987. *J. Geophys. Res.* 94, 11429-11436.

Krueger, A. J., 1983: Sighting of El Chichon sulfur dioxide clouds with the Nimbus 7 total ozone mapping spectrometer. *Science* 220, 1377-1379.

Labitzke, K., B. Naujokat, and M. P. McCormick, 1983: Temperature effects on the stratosphere of the April 4, 1982 eruption of El Chichon, Mexico. *Geophys. Res. Lett.* 10, 24--26.

Luhr, J. F., 1990: Experimental phase relations of water and sulfur-saturated arc magmas and the 1982 eruption of El Chichon volcano. *J. Petrology* 31, 1071.

Mackinnon, I. D. R., J.L. Gooding, D.S. McKay, and U.S. Clanton, 1984: The El Chichon stratospheric cloud: Solid particulate and settling rates. *J. Volcanol. Geotherm. Res.* 23, 125-146.

Matthews, E., 1983: Global vegetation and land-use: new high resolution data-bases for climate studies. *J. Climate Appl. Meteor.* 22, 474-487.

Newell, R. E., 1970: Stratospheric temperature change from the Mount Agung vol-

canic eruption. *J. Atmos. Sci.* **27**, 977-978.

Oberbeck, V. R., E.F. Danielsen, K.B. Snetsinger, and G. V. Ferry, 1983: Effect of the eruption of El Chichon on stratospheric aerosol size and composition. *Geophys. Res. Lett.* **11**, 1021-1024.

Oort, A. H., Global atmospheric circulation statistics, 1958-1973, NOAA *Professional Paper 14*, U.S. Department of Commerce, National Oceanic and Atmospheric Administration, Washington, D.C., April, 1983.

Palmer, K.F. and D. Williams, 1975: Optical constants of sulfuric acid; application to the clouds of Venus? *Appl. Optics* **14**, 208-219.

Parker, D.E. and J.K.L. Brownscombe, 1983: Stratospheric warming following the El Chichon volcanic eruption. *Nature* **301**, 406-408.

Peck, D. L., 1978: Cooling and vesiculation of Alae lava lake. USGS *Professional Paper 935B*, 59 pp.

Pollack, J. B., O.B. Toon, and B.N. Khare, 1973: Optical properties of some terrestrial rocks and glasses. *Icarus* **19**, 372-389.

Pollack, J. B., F.C. Witteborn, K. O'Brien, and B. Flynn, 1991: A determination of the infrared optical depth of the El Chichon volcanic cloud. *J. Geophys. Res.* **90**, 3115-3122.

Quiroz, R. S., 1983: The isolation of stratospheric temperature change due to the El Chichon volcanic eruption from nonvolcanic signals. *J. Geophys. Res.* **88**, 6773-6780.

Rampino, M. R., S. Self, and R.B. Stothers, 1988: Volcanic winters. *Ann. Rev. Earth Planet. Sci.* **16**, 73-99.

Rind, D., N. K. Balachandran, and R. Suozzo, 1992: Climate change and the middle

atmosphere, Part H: The impact of volcanic aerosols. *J. Climate* 5, 189–208.

Rosenfield, J. E., M.R. Schoeberl, and M.A. Geller, 1987: A computation of the stratospheric diabatic circulation using an accurate radiative transfer model. *J. Atmos. Sci.* 44, 859-876.

Rossow, W.B. and R.A. Schiffer, 1991: ISCCP cloud data products. *Bull. Amer. Meteor. Soc.* 72, 2–20.

Rothman, L. S., R.R. Gamache, R.H. Tipping, C.P. Rinsland, M.A.H. Smith, D.C. Benner, V.M. Devi, J.-M. Flaud, C. Camy-Peyret, A. Perrin, A. Goldman, S.T. Massie, C. It. Brown, and R.A. Toth, 1992: The HITRAN molecular database editions of 1991 and 1992. *J. Quant. Spectrosc. & Radiat. Transfer* 48, 469-507.

Rye, R.O, J.F. Luhr, and M.D. Wasserman, 1984: Sulfur and oxygen isotope systematics of the 1982 eruptions of El Chichon volcano, Chiapas, Mexico. *J. Volcan.* 23, 109-123.

Santee, M., 1992: The thermal structure, dust loading, and meridional transport in the Martian atmosphere during late southern summer. Ph.D. thesis, Calif. Inst. of Tech., 1992.

Santee, M. and D. Crisp, 1993: Thermal structure and dust loading of the Martian atmosphere during late southern summer: Mariner 9 revisited. *J. Geophys. Res.* 98, 3261-3279.

Santee, M. and D. Crisp, 1994: Diagnostic calculations of the circulation in the Martian atmosphere. Submitted to *J. Geophys. Res. - Planets*.

Shia, R. L., Y.L. Yung, M. Allen, R.W. Zurek, and D. Crisp, 1989: Sensitivity study

of advection and diffusion coefficients in a 2-dimensional stratospheric model using C-14 data. *J. Geophys. Res.* 94, 18467-18484.

Shibata, T., M. Fujiwara and M. Hirono, 1984: The El Chichon volcanic cloud in the stratosphere: lidar observations at Fukuoka and numerical simulation. *J. Atmos. Terrest. Phys.* 12, 1121-1146.

Stamnes, K., S.-C. Tsay, W. Wiscombe, and K. Jayaweera, 1988: Numerically stable algorithm for discrete-ordinate method radiative transfer in multiple-scattering and emitting layered media. *Appl. Optics* 27, 2502-2509.

Thekaekara, M. P., 1969: Solar fluxes at the top of earth's atmosphere. *Appl. Opt.* 8, 1713-1732.

Thomas, G. E., B.M. Jakosky, R.A. West, and R.W. Sanders, 1983: Satellite limb-scanning thermal infrared observations of the El Chichon stratospheric aerosol: First results. *Geophys. Res. Lett.* 10, 997-1000.

Turco, R. P., O.B. Toon, R.C. Whitten, P. Hamill, and R.G. Keese, 1983: The 1980 eruptions of Mt. St. Helens: physical and chemical processes in the stratospheric cloud. *J. Geophys. Res.* 88, 5299-5319.

Vupputuri, R.K.R. and J.P. Blanchet, 1984: The possible effects of El Chichon eruption on atmospheric thermal and chemical structure and surface climate. *Geof. Int.* 23, 433-447.

Warneck, P., 1988: *Chemistry of the Natural Atmosphere*. San Diego, Academic Press, 757 pp.

Warren, S. G., 1982: Optical properties of snow. *Rev. Geophys.* 20, 67-89.



Wilson, L. and T.C. Huang, 1979: The influence of shape on the atmospheric settling velocity of volcanic ash particles. *Earth Planet. Sci. Lett.* 44, 311-324.

Wiscombe, W. J., 1980: Improved Mie-scattering algorithms. *Appl. Optics* 19, 1505-1509.

World Meteorological Organization, 1986: *Atmospheric Ozone 1985*. WMO Global Ozone Research and Monitoring Project Report No. 16, Vol. I.

Young, R. E., H. Houben, and O.B. Toon, 1994: Radiatively forced dispersion and induced temperature perturbations in the stratosphere during the first few months following the eruption. *Geophys. Res. Lett.* 21, 369-372.

(near text  
page 19)

Table I					
Stokes Fall Time (in Days) from 26 km					
R (um)	0.2	0.6	1.0	3.0	5.0
to 21 km	730	81.	29.	3.2	1.2
to tropopause	1428	159	57.	6.3	2.3

Fig. 1 Above: diurnal average radiative heating rates for a typical July climate at 20°N, with a clear sky (solid curve) and with a sulfuric acid aerosol layer (dashes) as described in the text. Below: short-wave (solid) and long-wave (dashes) components of the difference between the aerosol heating rate and the clear-sky heating rate.

Fig. 2 Above: streamfunction of the meridional circulation for a typical July climate with only tropospheric water clouds. Units arc 100 m<sup>2</sup>/s, intervals 1000 m<sup>2</sup>/s. Below: the same, with a sulfuric acid aerosol layer as described in the text.

Fig. 3 Absorption cross-sections of ozone (dashes) and sulfur dioxide (solid) at ultra-violet and visible wavelengths, derived from Demore et al (1992).

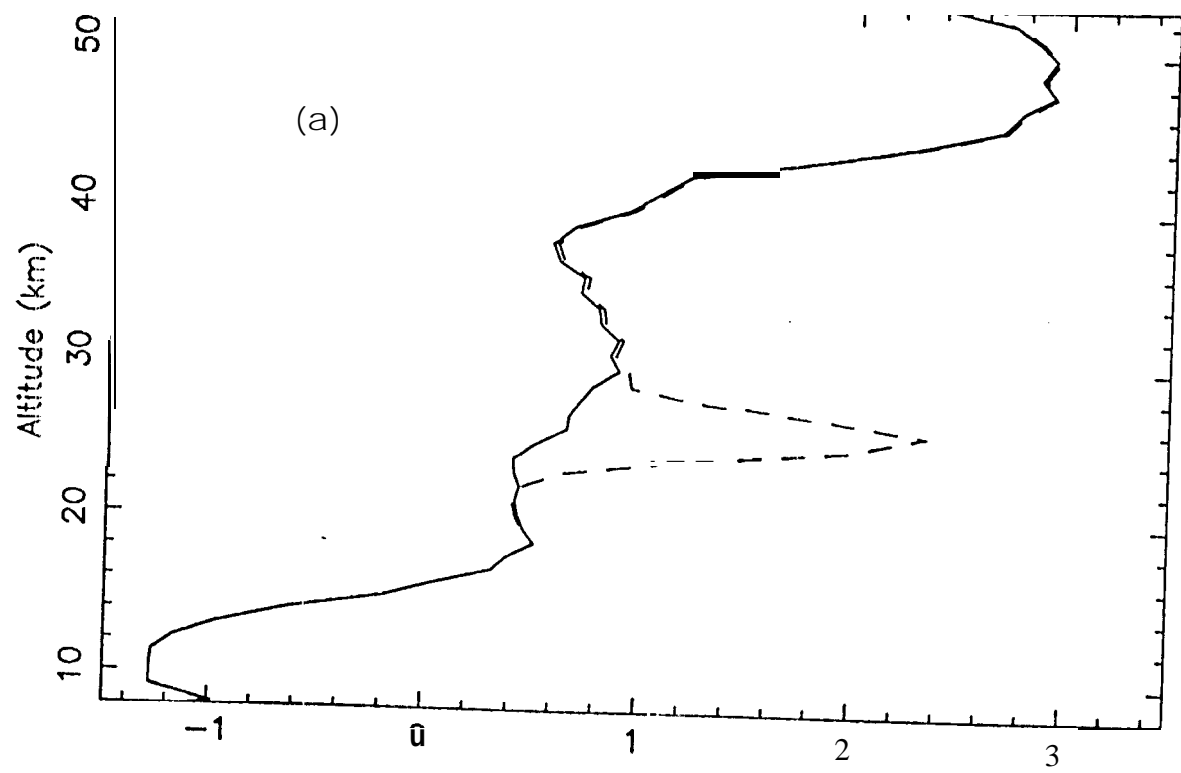
Fig. 4 Diurnal average radiative heating rates for a typical April climate with a sulfur dioxide layer (100 DU) centered at 34 km, 26 km, 16 km (all dashes); 30 km, 22 km, 10 km (all solid).

Fig. 5 Diurnal average radiative heating rate at the peak of a sulfur dioxide layer centered at 26 km altitude. The heating rate is shown as a function of the total column amount of sulfur dioxide. Dashes: total heating for a 7-gas atmosphere including the volcanic sulfur dioxide layer. Dots: excess over the typical April net heating at 26 km altitude with unperturbed sulfur dioxide. Graph begins at 15 DU, our threshold for

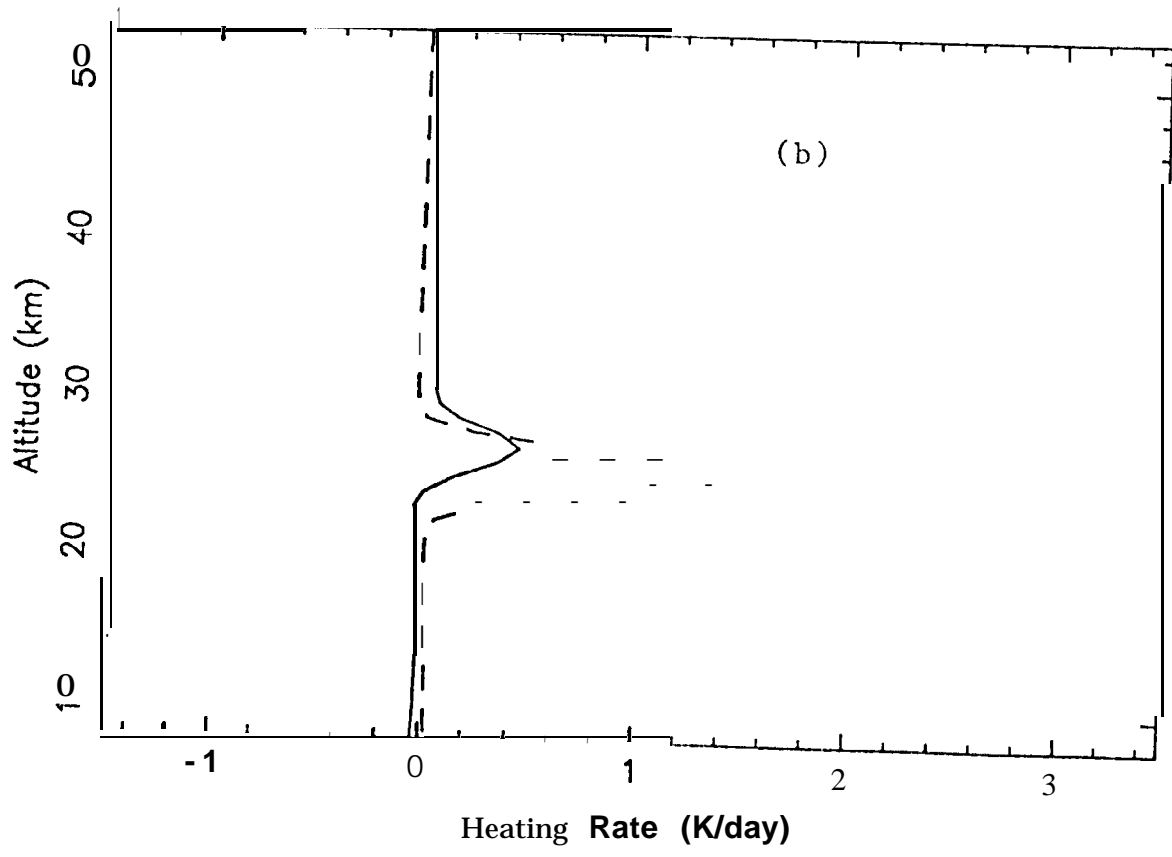
recognizing perturbed  $\text{SO}_2$  in the TOMS data,

Fig. 6 Above: diurnal average radiative heating rate profile for a typical April atmosphere after injection of an ash layer described in the text,  $\tau = 0.6$  in each case. In the range of particle radii shown, the peak heating rate increases monotonically with particle size. Mean radii of 1  $\mu\text{m}$  (dashes), 3  $\mu\text{m}$  (solid), 5  $\mu\text{m}$  (dot-dash). Below: Short-wave (solid) and long-wave (dashes) components of the difference between 3pm ash heating and clear-sky heating. Ash optical properties in all cases are those of crystalline andesite.

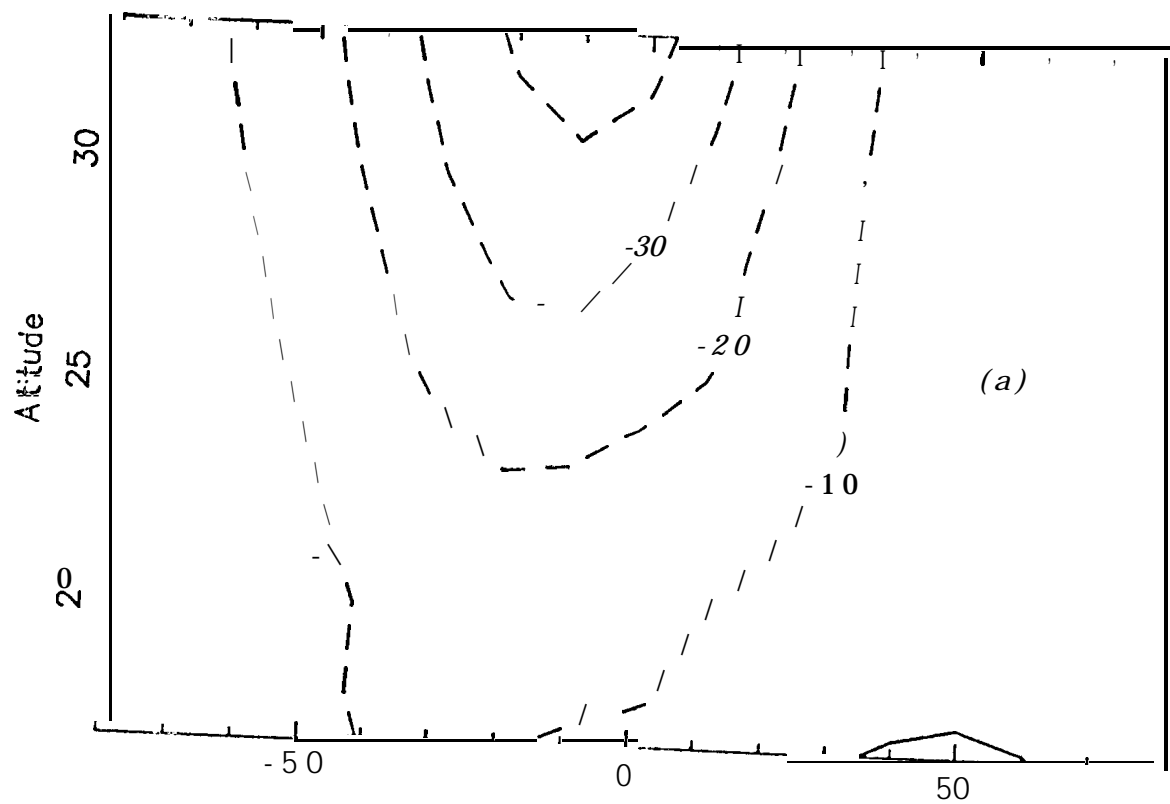
Fig. 7 Above: streamfunction of the meridional circulation for a typical April climate with only tropospheric water clouds. Units are  $100 \text{ m}^2/\text{s}$ , intervals  $1000 \text{ m}^2/\text{s}$ . Below: the same, after injection of a layer of 3- $\mu\text{m}$  andesite dust particles as described in the text.



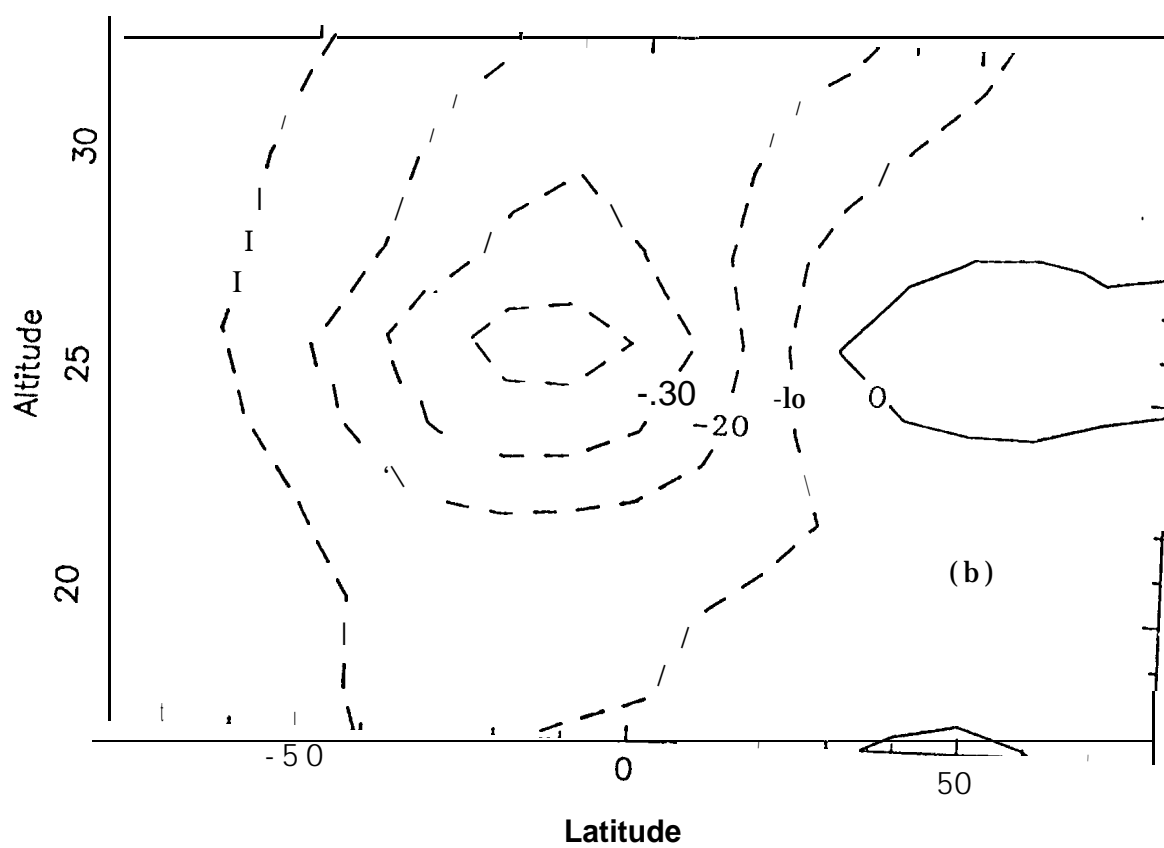
SW and LW aerosol htg effect

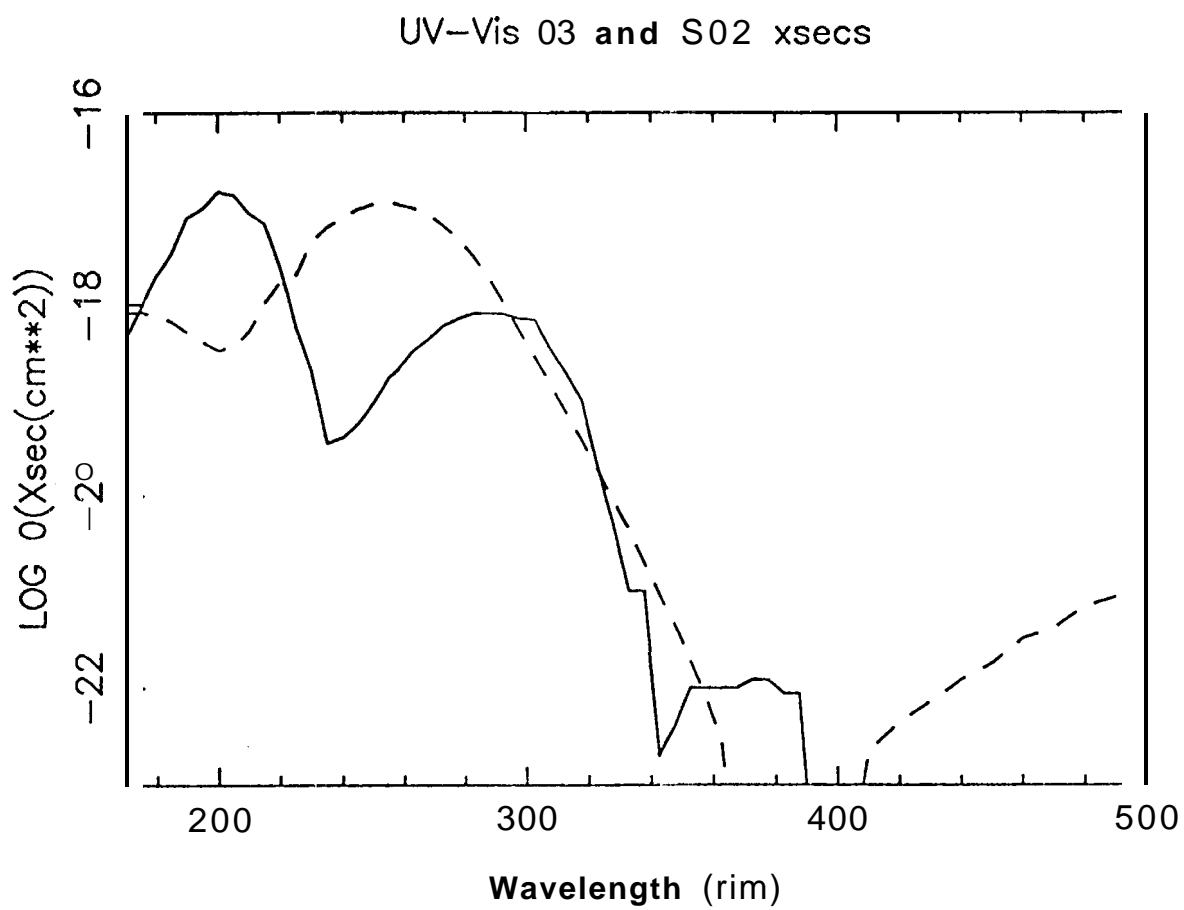


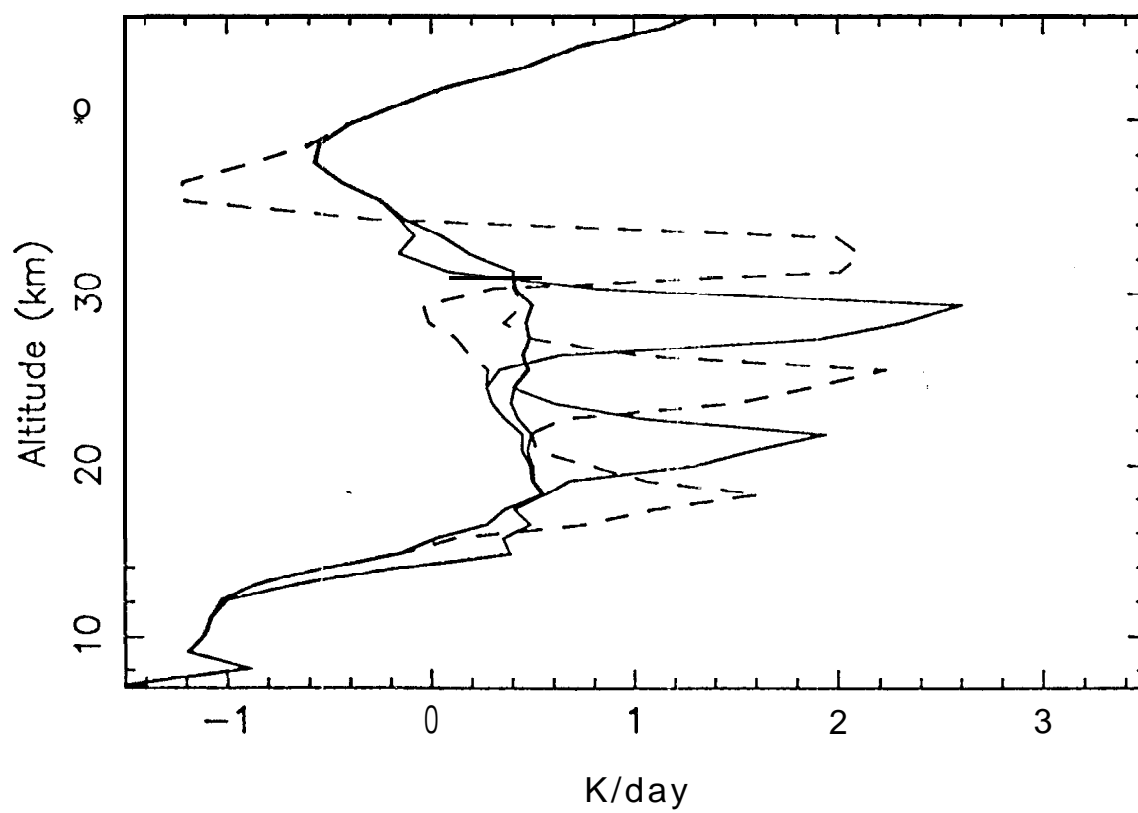
July streamfunction, clear stratosphere



July streamfunction w/ aerosol layer

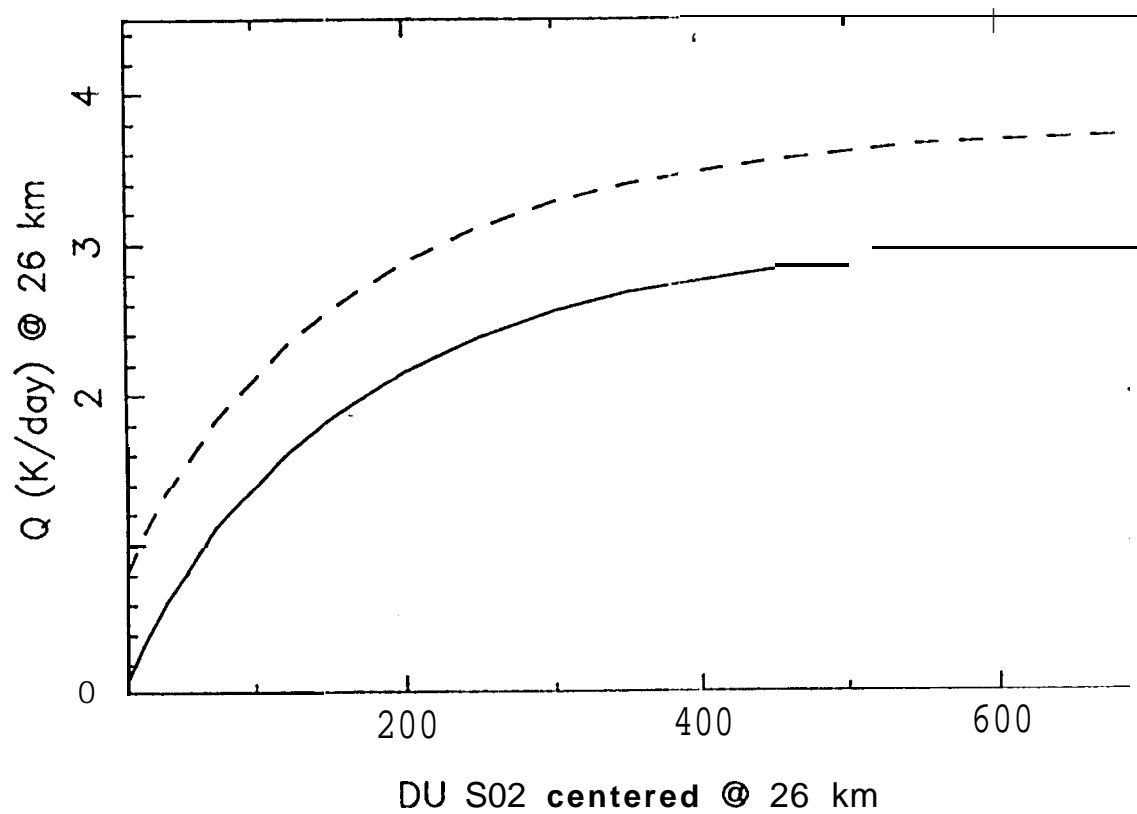




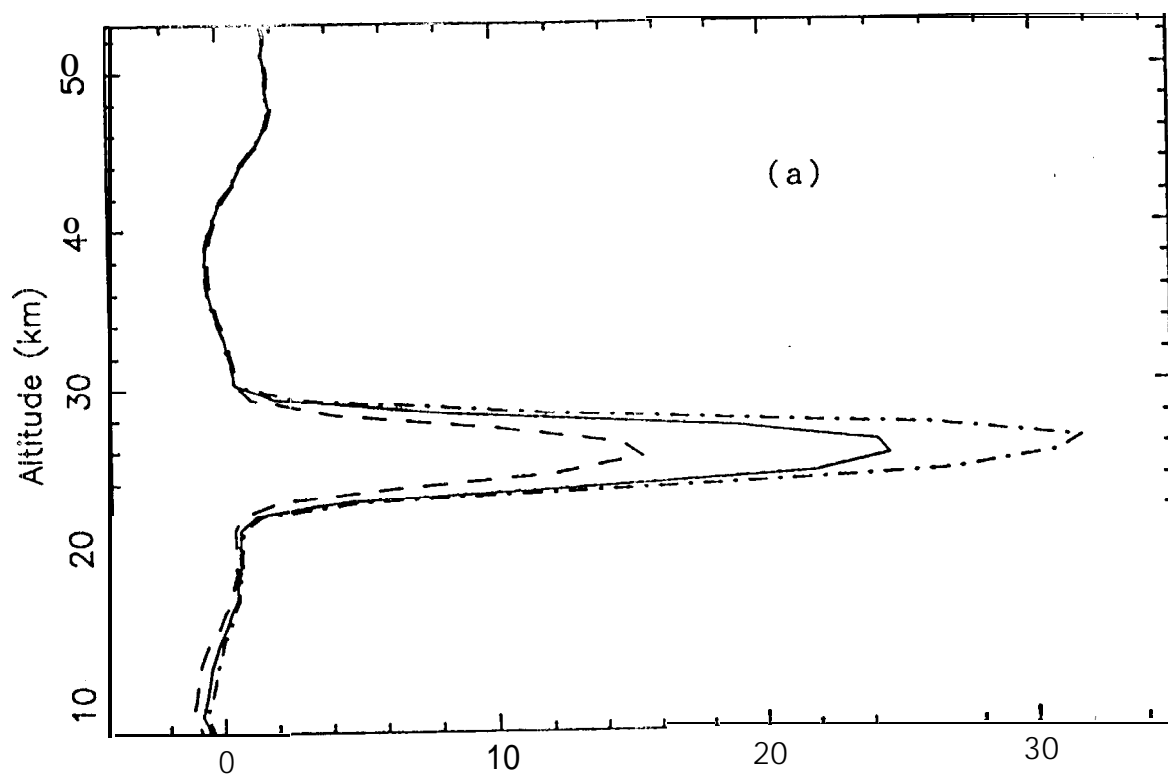
Q vs. altitude of SO<sub>2</sub> layer



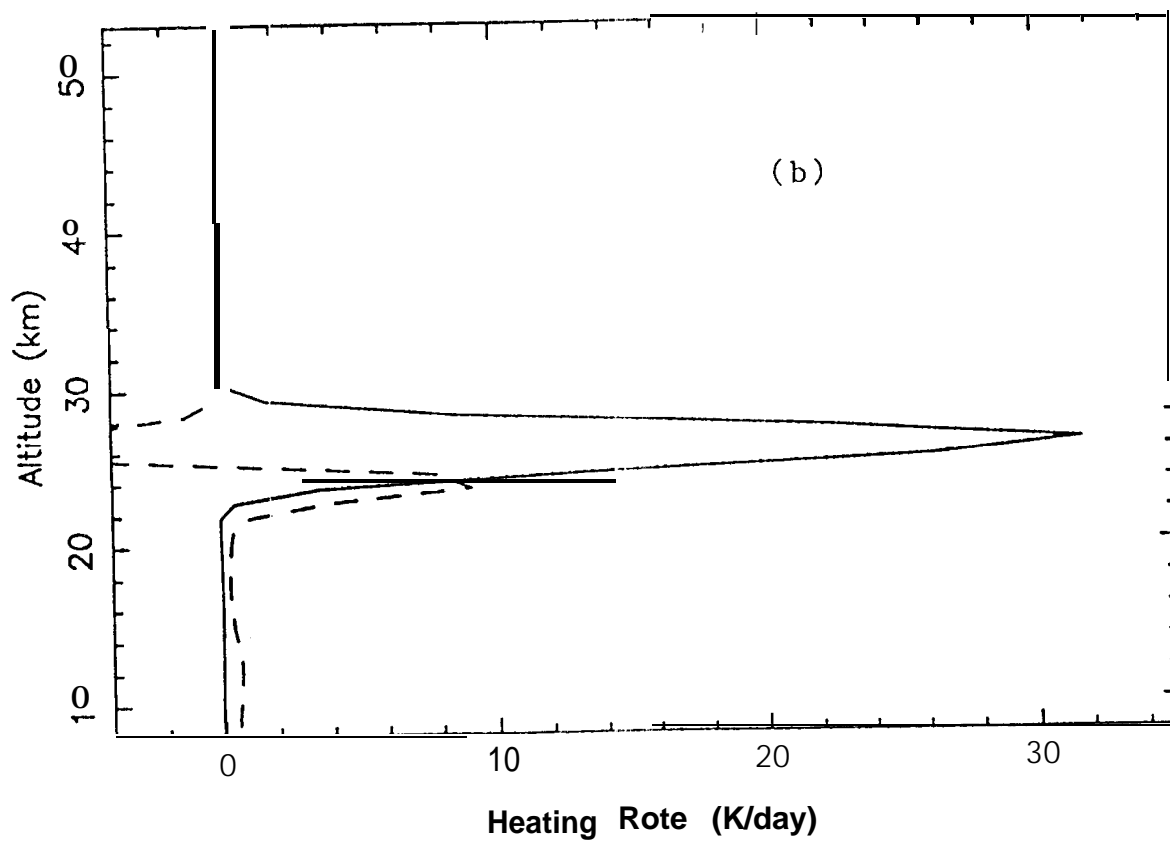
Q vs. S02 column amt



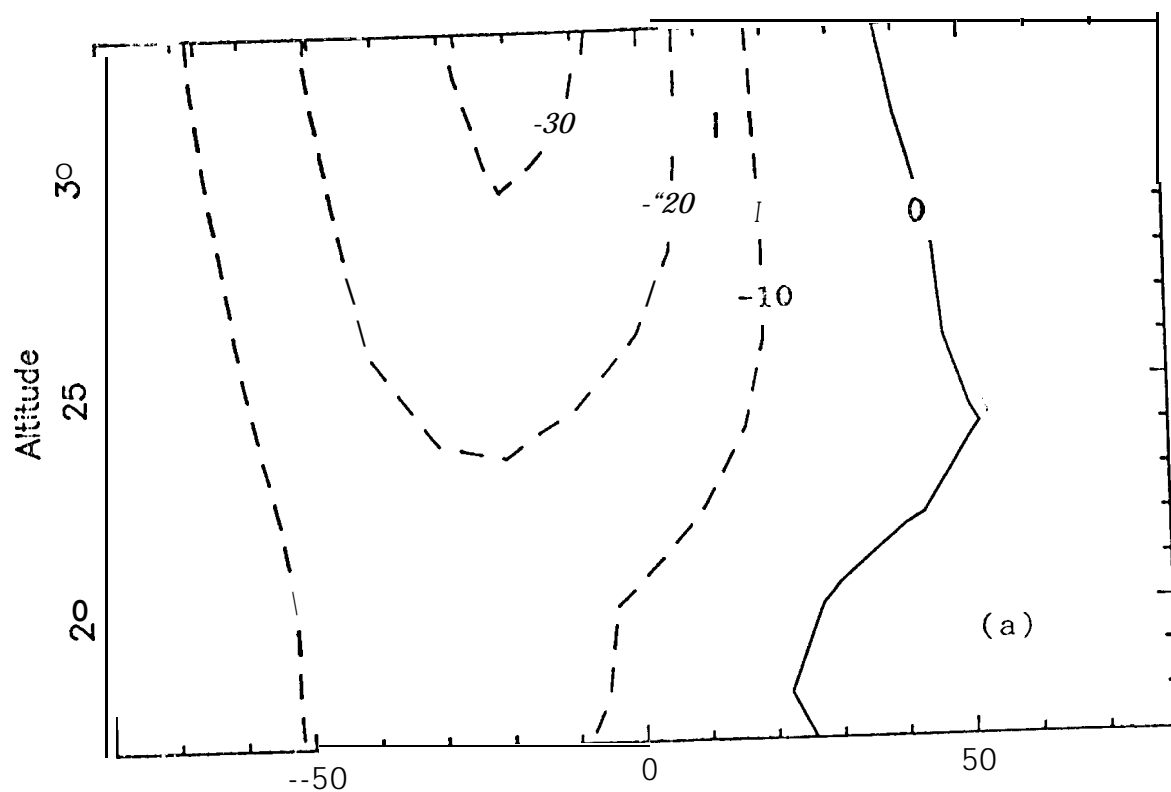
Q vs. silicate ash size



SW and LW silicate ash htg



April streamfunction, water clouds only



April streamfunction w/ 3um ash layer

